The surface states of transition metal X-ides under electrocatalytic conditions

The Surface States of Transition Metal X-ides under Electrocatalytic Conditions

Heng Liu [a, b], Xue Jia [a], Ang Cao [d], Li Wei [e,], Carmine D'agostino [b,c,*], and Hao Li [a,*]*

[a] *Advanced Institute for Materials Research (WPI-AIMR), Tohoku University, Sendai 980-8577, Japan*

[b] *Department of Chemical Engineering, The University of Manchester, Oxford Road, M13 9PL, UK*

[c] *Dipartimento di Ingegneria Civile, Chimica, Ambientale e dei Materiali (DICAM), Alma Mater Studiorum – Università di Bologna, Via Terracini, 28, 40131 Bologna, Italy*

[d] *Catalysis Theory Center, Department of Physics, Technical University of Denmark, 2800 Lyngby, Denmark*

[e] *School of Chemical and Biomolecule Engineering, The University of Sydney, Darlington 2006, NSW, Australia*

*** Correspondence:**

l.wei@sydney.edu.au (L.W.)

carmine.dagostino@manchester.ac.uk (C.D.)

li.hao.b8@tohoku.ac.jp (H.L.)

Abstract

Due to the conversion equilibrium between solvent and H- and O-containing adsorbates, the true surface state of a catalyst under a particular electrochemical condition is often overlooked in electrocatalysis research. Herein, by using surface Pourbaix analysis, we show that many electrocatalytically active transition metal X-ides (*e.g.*, oxides, nitrides, carbides, and hydroxides) tend to possess the surface states different from their pristine stoichiometric forms under the pH and potential of interests due to water dissociation or generation. Herein, summarizing the density functional theory calculated surface Pourbaix diagrams of fourteen conditionally stable transition metal X-ide materials, we found that some of these surfaces tend to be covered by O-containing adsorbates at a moderate or high potential, while vacancies or H-covered surfaces may form at a low potential. These results suggest the possibility of poisoning or creation of surface sites beyond the pristine surface, implying that the surface state under reaction conditions (pH and potentials) needs to be considered before the identification and analysis of the active sites of a transition metal X-ide catalyst. In addition, we provide an explanation of the observed theory and experiment discrepancy that some transition metal X-ides are "more stable in experiment than in theory". Based on our findings, we conclude that analyzing the surface state of transition metal X-ide electrocatalysts by theoretical calculations (*e.g.*, surface Pourbaix diagram analysis), *in-situ*/*operando* and post-reaction experiments are indispensable to accurately understanding the catalytic mechanisms.

Keywords: surface state; transition metal X-ides; surface Pourbaix diagram; electrocatalysis.

Maintext

Electrocatalysis is one of the keys to realizing a sustainable future.[1] By integrated electrocatalytic techniques, inexpensive feedstocks can be converted into value-added products powered by the green electricity generated from renewable sources (*e.g.*, wind, tide, and solar energy). This strategy can potentially revolutionize the non-renewable resources based industrial processes. To date, some electrocatalytic reactions have been widely studied, including hydrogen evolution reaction (HER),[2,3] oxygen evolution reaction (OER),[3] oxygen reduction reaction (ORR),[4] CO_2 reduction reaction (CO_2RR),[5] and nitrogen reduction reaction (NRR).[6] However, though some precious metal-based catalysts showed high performance at operating conditions for these reactions (*e.g.*, Pt and Pd for HER and ORR,[2,4] Ir and Ru for OER,[3] Au and Ag for CO_2RR,[7,8] and Ru for NRR[9,10]), the high price seriously hamper their further applications. To ensure a broader application of electrocatalysis in industry, exploiting stable and active catalysts with less reliance on expensive elements is a sought-after goal.

Non-precious transition metal X-ides (or, in brief: X-ides, including oxides, nitrides, carbides, sulfides, phosphides, hydroxides, and their derivatives) are a class of promising and low-cost alternatives to precious metal-based catalysts because of the experimentally proven stability under various electrocatalytic conditions,[11,12] especially in alkaline media. So far, some transition metal oxides (TMOs) have been found stable in acidic conditions under a wide range of potentials.[12–14] A recent data-mining study further proved that there existed some non-precious TMOs that could be thermodynamically stable under acidic oxygen electrocatalysis conditions.[15] Compared to acidic media, much more X-ides can survive in an alkaline electrocatalytic environment.[16] Recent development of anion exchange membrane fuel cell, which can operate under alkaline conditions, allows for a broader range of stable X-ides to be considered for oxygen electrocatalysis materials. For example, zirconium nitride (ZrN), a typical non-precious metal-based X-ide, was found to be highly active and stable under ORR potentials in alkaline media, with the ORR performance even comparable to Pt.[17] Because of their low-cost and conditionally stable properties, X-ides became a hot research spot in recent years.[18]

As the number of X-ides research increases rapidly, the demand for understanding the surface science (*e.g.*, the adsorption and reaction mechanism at a surface) of X-ides also dramatically increases. Rational design guidelines for high-performance X-ides are urgently needed to provide reliable suggestions for experiments to reduce the conventional trial-and-error process in searching the promising X-ides for target electrocatalysis. Therefore, theoretical *ab initio* computations, primarily based on density functional theory (DFT),[19] are widely used to calculate the reaction kinetics and thermodynamics of an electrocatalytic reaction on a defined X-ide surface. Based on the calculated kinetics and thermodynamics, key information (*e.g.*, active sites) and design guidelines for new catalysts can be acquired through scaling relation analysis and microkinetic modeling.[20] These theoretical insights can significantly promote the development of promising X-ide electrocatalysts.

A key challenge of such technique is that the true surface states of X-ides under electrocatalytic conditions are not clear. Many mechanistic and active-site analysis reported to date were based on a pristine stoichiometric surface cleaved from a bulk structure, while catalytic *in-situ* or post-reaction characterizations on X-ide catalysts were usually dismissed in experimental works. However, the dynamic equilibria between water and H- and O-containing surface adsorbates (*via* the reactions: $H_2O + * \leftrightarrow HO^* + e^- + H^+$ and $H_2O + * \leftrightarrow O^* + 2e^- + 2H^+$, where $*$ represents a surface site) could lead to the existence of adsorbate pre-coverage or vacancy formation on the surface. In other words, the X-ide surfaces may either be occupied by additional cations/anions originating from the liquid phase dissociation or the formation of anion vacancy through O* or HO* protonation, suggesting a "true" catalyst surface under electrochemical conditions state may deviate significantly from its stoichiometric state.

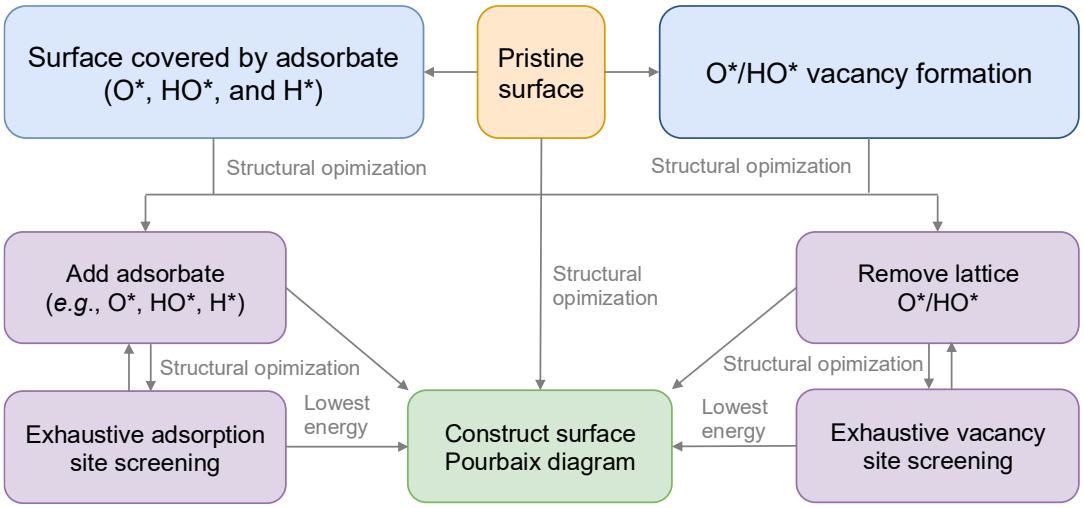

Figure 1. Flow chart of developing a surface Pourbaix diagram for surface state analysis. Starting from a pristine surface, exhaustive DFT calculations on the Gibbs free energies of the surfaces with additional O*/HO*/H* adsorbate and with O*/HO* vacancy formation will be performed. For each coverage, all possible sites are in principle needed to be sampled and the lowest energy one should be selected for surface Pourbaix diagram construction. Afterwards, the surface Pourbaix diagram as a function of pH and potential will be derived to unravel the surface state of the surface under various pH and potentials.

Surface Pourbaix diagram with the calculated Gibbs free energies of different surface states as a function of pH and operating potential first proposed by Hansen et al. in 2008,[21] is essential to analyze the thermodynamically favorable surface state under electrochemical conditions. Details of the computational methods of surface Pourbaix diagram are shown in the **Supplementary Materials**. This method has shown predictive power in analyzing the surface coverage of electrocatalysts. The flow chart of developing a surface Pourbaix diagram is shown in **Figure 1**. For example, Vinogradova et al.[22] found that Pt (111), the most widely studied ORR catalyst, was covered by ~1/3 HO* under ORR potentials, in good agreement with the *in-operando* experimental observations.[23] Yang et al.[24] found that most of the emerging metal-nitrogen-carbon (M-N-C) dual-atom catalysts

(DACs) with 6N/C-coordination were poisoned by O* even at a low reversible hydrogen electrode (RHE) potential, which is due to the presence of the strong-O-binding metal-metal bridge site. Zhou et al.[25] found that the (111) and (110) surfaces of an emerging acid-stable ORR catalyst, $CoSb_2O_6$, is in part covered by H* at the surface lattice oxygen sites under ORR potentials in acid. Zhu et al.[26] found that two-dimensional metal borides (MBenes), including Mo_2B_2, Ti_2B_2, and Cr_2B_2, would undergo a significant oxidation even at a negative potential *vs*. RHE. Very recently, Pan et al.[27] found that the (101) surfaces of $Mn_8O_{10}Cl_3$ and $Mn_{7.5}O_{10}Br_3$ would undergo a significant electrochemical oxidation at OER potentials, with the surfaces additionally covered by >0.5 monolayer (ML) O*, in excellent agreement with their post-catalysis X-ray photoelectron spectroscopy (XPS) and X-ray absorption near-edge spectroscopy (XANES) characterizations. This self-oxidation process leads to a passivated layer that prevents Mn ions from leaching out and, meanwhile, leads to the formation of highly active Mn-sites for OER. This also explains why $Mn_8O_{10}Cl_3$ and $Mn_{7.5}O_{10}Br_3$ in their pristine forms do not seem to be stable from phase diagrams but in fact they are highly stable under low-pH, oxidative OER conditions. All these examples show that many less close-packed catalysts, especially X-ides surfaces, may have very different surface states compared to their pristine forms. Unfortunately, regardless of the success of using surface Pourbaix analysis to unravel the surface state information, the importance of this analytical method is generally dismissed.

Motivated by the above, herein, we perform case studies on the electrochemical states of some typical surfaces of X-ide catalysts and their derivatives, including TMOs (and TMOs-derivatives with some common structures, perovskite, spinel, and rutile) like RuO_2, IrO_2, RhO_2, NiO, β-MnO_2, $LaMnO_3$, Sb_2WO_6, $Co_2Mo_3O_8$, $ZnCr_2O_4$, $LaPO_4$, and $Ti_3C_2O_2$, transition metal nitride (ZrN), transition metal carbide (MoC), and transition metal hydroxide (NiFe layered double hydroxide, LDH) (**Figure 2**). Details of the computational and modeling methods are shown in the **Supplementary Materials**. All these analyses are based on the computational hydrogen electrode (CHE) method developed by Nørskov et al.[28] All these materials were proven stable under some specific electrocatalytic environments based on either experimental or theoretical analyses.[17,29–50] for example, β-MnO_2, $LaMnO_3$, Sb_2WO_6, $Co_2Mo_3O_8$, $LaPO_4$, $Ti_3C_2O_2$, ZrN, and NiFe LDH can be stable at ORR or OER conditions, while NiO, $ZnCr_2O_4$, and MoC are stable at relatively reducing conditions (*e.g*., HER and NRR). For each material, the facet with a low surface energy was selected for analyses (**Tables S1-S6**). For each state (*i.e*., the line) of a surface Pourbaix diagram, we performed exhaustive computational screening on the potential sites and adsorption geometries and discarded the identified high-energy states; only the most energetically favorable states were plotted. Since the precise computation of protonation/deprotonation energetics under different pH demands a thorough consideration of the electric field effects[51] and is limited by the computationally expensive kinetic barrier calculations for water dissociation with explicit models which, it is still an open question to integrate these effects into surface Pourbaix diagram calculations. Herein, all the surface Pourbaix diagrams generated in this study at an RHE scale were based on the hypothesis that many of the kinetic barriers of water dissociation can be overcome at the potential of interests which is discussed by the pioneering works of Chan et al.[52,53] and thus we

suspect that pH does not lead to a qualitative difference in our computed results concerning the trends of coverage under working conditions. Moreover, the solvation effect was taken into account. The molecular dynamics simulation results using explicit solvation models on an IrO_2(110) surface was previously introduced to account for the solvation effect with a correction value of ~-0.15 and ~0 eV for HO* and O*, respectively.[54] Considering that the solvation effects mainly originate from the hydrogen-bonding between the hydroxyl and the water molecules, different TMX materials may share a similar solvent effect. Therefore, all calculations relating the formation of HO* (including both the direct generation of HO* and the protonation at the O*-site) were considered with a solvation correction of a value as an approximation. Based on the results from the computed surface Pourbaix diagrams, we did further investigation on the catalytic activity for each reaction on its most favorable surface under corresponding reaction conditions (specific pH value and potential). The adsorption energy of respective key intermediate was calculated to represent the activity. In details, these intermediates are H_2O* for HER, O* and HO* for OER, HO* for ORR, COOH* for CO_2RR, and NNH* for NRR. For comparison, the relevant adsorption energy on the pristine surface for the species above was also computed. Furthermore, the scaling relation analysis was also introduced to give a deeper insight about the importance of determining the surface state of X-ides for each specific reaction condition.

Summarizing the surface Pourbaix diagrams of the fourteen conditionally stable transition metal X-ide materials based on DFT calculations with a sufficient level of accuracy for each system (**Figure 2**), we found that at a moderate or high potential (*e.g.*, U_{RHE} >0 V), some of these surfaces tend to be covered by O-containing molecules, while vacancy-containing or H-covered surfaces may form at a low potential. These results suggest the possibility of surface site poisoning or creation beyond the pristine surface, implying that the surface state under reaction pH and potentials needs to be defined before assigning the active sites of a transition metal X-ide catalyst. Note that we herein aim to provide essential examples to illustrate the importance of surface state analysis, while constructing a surface Pourbaix diagram requires exhaustive computations; it is likely that there are other even more favorable surface states that are yet to be identified. Nevertheless, this will not alter our conclusion since most of the favorable surface states identified so far are already beyond their pristine forms. To develop a full surface Pourbaix diagram, improved computational methods (*e.g.*, machine learning guided methods)[55] need to be developed. To further analyze their corresponding surface states at different electrocatalytic scenarios and the corresponding reaction activity, the characteristic potentials for various reactions were selected in the consideration of overpotential. Herein, due to the variety of working potentials of each electrocatalysis, we focus on the potential examples which have been proven suitable as the references,[24] *i.e.*, 1.60 V_{RHE} for OER,[56] 0.78 V_{RHE} for ORR,[57] -0.10 V_{RHE} for HER,[58] −0.35 V_{RHE} for CO_2RR,[59] and −0.40 V_{RHE} for NRR.[60]

As tabulated in **Table 1**, we can clearly see that most of the ORR- or OER-active X-ides (β-MnO_2, $LaMnO_3$, W-Sb-O, $Co_2Mo_3O_8$, $LaPO_4$, $Ti_3C_2O_2$, and ZrN) tend to be covered by O* or HO*, expect for NiFe LDH where hydroxyl vacancy will be formed. All these are in excellent agreement with some post-catalysis experimental

observations that most of these catalysts will undergo an electrochemical oxidation process,[36] while NiFe LDH will form oxygen vacancies even at OER conditions.[39]

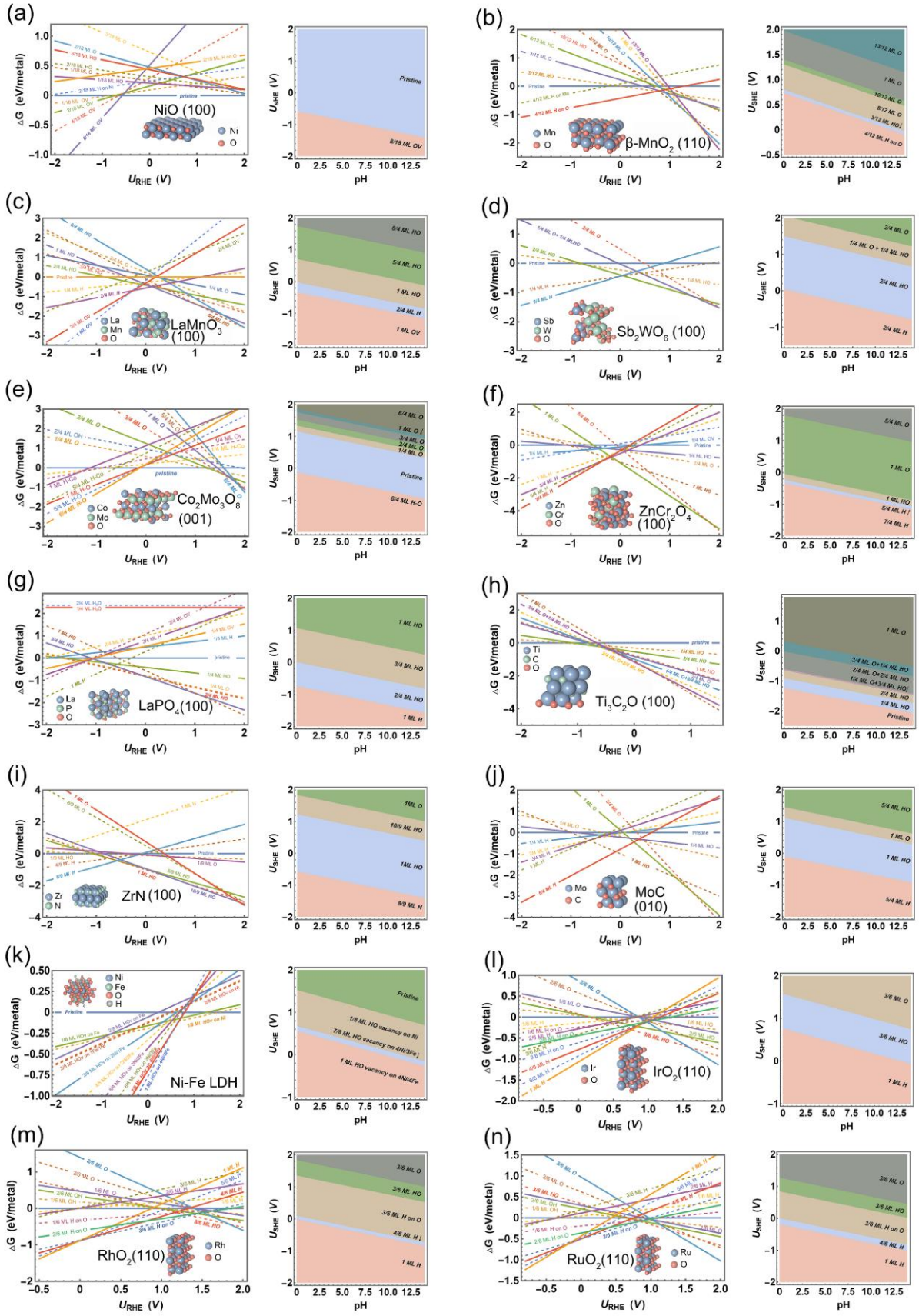

Figure 2. Calculated 1D and 2D surface Pourbaix diagrams of the fourteen typical X-ide surfaces for electrocatalysis as a function of pH and potential. Insets show the pristine surfaces of these structures in which oxygen was denoted by red. Specifically, NiO (a), β-MnO_2 (b), $LaMnO_3$ (c), Sb_2WO_6 (d), $Co_2Mo_3O_8$ (e), $ZnCr_2O_4$ (f), $LaPO_4$ (g), Ti_3C_2O (h), ZrN (i), MoC (j), NiFe-LDH, HO_v (denotes HO vacancy) (k), IrO_2 (l), RhO_2 (m), and RuO_2 (n). The high-energy states beyond the *y*-scale are not shown in the plots. The magnified pictures of the sub-figures are shown in **Figures S1-S14**.

Taking the typical RuO_2 as an example, our results found that all the Ru in CUS (coordinatively unsaturated site) are covered by O* during OER, which can be proven by Rao et al.[61] both theoretically and experimentally. The results that all bridge site Ru in RuO_2 will be occupied by HO* under ORR potentials also aligns with the Pourbaix diagram results generated by Abbott et al.[41] Exclusively, in addition to considering more comprehensive coverage cases, the solvation effect was also considered in this work. At the potentials of interest of HER, CO_2RR, and NRR, many of these catalysts tend to form O-vacancy or are covered by H*. Note that due to the variety of overpotentials, an even more negative potential is sometimes required to proceed CO_2RR or NRR.[29–31] For NiO, O-vacancy formation could be more favorable when the potential is below −0.50 V_{RHE} (**Figure 2a**). Notably, some recent experiments identified that the oxygen vacancy sites of NiO(100) can be highly active for NRR, leading to the formation of strong-binding Ni four-fold hollow sites that are highly active in N-adsorption and N ≡N activation.[29] To clarify, although structural reconstruction may happen in the bulk phase of materials like NiO under a high potential, here our study is based on the NiO surface motivated by its activity in ammonia synthesis which happens at a very low potential rather than an oxidic potential. On the other hand, the result showing the surface of NiO is totally different from the pristine one under potential of interest can also demonstrate the further intrinsic reconstruction. All these results clearly show that at these common electrocatalytic reactions, the surface states of X-ides can be very different from their pristine surfaces, and that we should pay particular attention to analyzing the surface state before activity and product-selectivity exploration. In addition, we herein bring up the concept of the electrochemical potential window (EPW, as shown in **Table 1**), which was first defined by Yang et al.[24] for dual-atom electrocatalysts: the potential range that the X-ide surface can remain pristine. Interestingly, most of the surfaces of interests here possess a very narrow EPW, while many of them even do not possess such a window to exhibit a pristine surface.

Table 1. Corresponding surface states of the eleven X-ides at the selected characteristic potentials of HER (-0.10 V_{RHE}), OER (1.60 V_{RHE}), ORR (0.78 V_{RHE}), CO_2RR (−0.35 V_{RHE}), and NRR (−0.40 V_{RHE}).

Materials	Electrochemical potential window (V)	HER (-0.10 V_{RHE})	OER (1.60 V_{RHE})	ORR (0.78 V_{RHE})	CO_2RR (-0.35 V_{RHE})	NRR (-0.40 V_{RHE})
NiO	−0.8 ~2	Pristine	Pristine	Pristine	Pristine	Pristine

β-MnO_2	N/A	4/12 ML H*	1 ML O*	3/12 ML HO*	4/12 ML H*	4/12 ML H*
$LaMnO_3$	N/A	2/4 ML H*	5/4 ML O*	1 ML HO*	1 ML O Vacancy	1ML O Vacancy
Sb_2WO_6	N/A	2/4 ML H*	1/4 ML O*+1/4 ML HO*	2/4 ML HO*	2/4 ML H*	2/4 ML H*
$Co_2Mo_3O_8$	-0.1-1.2	Pristine	3/4 ML O*	Pristine	6/4 ML H* on O	6/4 ML H* on O
$ZnCr_2O_4$	N/A	1 ML HO*	1 ML O*	1 ML O*	5/4 ML H*	7/4 ML H*
$LaPO_4$	N/A	2/4 ML HO*	1 ML HO*	3/4 ML HO*	2/4 ML HO*	2/4 ML HO*
Ti_3C_2O	−2 ~ −1.3	3/4 ML O*+1/4 ML HO*	1 ML O*	1 ML O*	2/4 ML O*+2/4 ML HO*	2/4 ML O*+2/4 ML HO*
ZrN	N/A	1 ML HO*	10/9 ML HO*	1 ML HO*	1 ML HO*	1 ML HO*
MoC	N/A	5/4 ML H*	5/4 ML O*	1 ML HO*	5/4 ML H*	5/4 ML H*
NiFe LDH	1.5 ~2	1 ML HO Vacancy	Pristine	1/8 ML HO Vacancy	1 ML HO Vacancy	1 ML HO Vacancy
IrO_2	N/A	1 ML H*	3/6 ML O*	3/6 ML HO*	1 ML H*	1 ML H*
RhO_2	N/A	1 ML H*	3/6 ML HO*	3/6 ML H* on O	1 ML H*	1 ML H*
RuO_2	N/A	4/6 ML H*	3/6 ML O*	3/6 ML H* on O	1 ML H*	1 ML H*

Based on these results, we can further comment on the surface stability of some X-ides under specific electrocatalysis. For example, from bulk Pourbaix diagram calculations (as illustrated in the Materials Project[62] database), ZrN is known to be unstable in alkaline ORR conditions. However, it is proven to be highly stable and ORR-active in experiments.[17] From the surface Pourbaix diagram calculations in this work (**Figure 2i**), we found that a ZrN surface is fully oxidized at the potential >-0.5 V_{RHE}. Given that ZrO_x is known to be kinetically stable, and it has been proved as an acid-stable ORR TMO catalyst,[13,14,63] this self-oxidation phenomenon identified that the ZrN surface could prevent the surface cation from leaching out. This phenomenon is somewhat similar to the

self-oxidation process identified by Pan et al.[27] when explaining the high acidic stability of Mn-based oxides for OER. In addition, these surface Pourbaix analyses also testify the availability of the design concept of X-ides as the "pre-catalysts" for OER,[64,65] where a self-oxidation was observed at OER conditions, and the active-phases of many X-ides were proven to be a significantly oxidized surface instead of the as-synthesized surface. To note, a different surface state would also lead to changes in the interfacial properties of a catalyst, such as the potential of zero-charge and the surface hydrophobicity, which will contribute to the catalytic mechanism being different from a pristine surface.

Table 2. Adsorption energy for different key intermediates under relevant reaction conditions on pristine- (Pri) and relevant covered-surface (Cov). The difference of the Gibbs free energy is also given as ΔΔG. The considered potentials for these five reactions are the same with **Table 1**. N/A means that the surface is poisoned or physical-adsorption-dominated.

Materials	G_{H2O} (HER) eV			G_O-G_{HO} (OER) eV			G_{HO} (ORR) eV			G_{COOH} (CRR) eV			G_{NNH} (NRR) eV		
	Pri	Cov	ΔΔG	Pri	Cov	ΔΔG	Pri	Cov	ΔΔG	Pri	Cov	ΔΔG	Pri	Cov	ΔΔG
NiO	0.91	N/A	N/A	0.82	N/A	N/A	3.37	N/A	N/A	2.92	N/A	N/A	3.99	N/A	N/A
β-MnO_2	-2.21	-0.13	2.08	0.7	0.58	-0.12	-0.8	1.07	1.87	1.5	2.57	1.07	0.54	2.36	1.82
$LaMnO_3$	2.35	-0.5	N/A	1.41	1.78	0.37	-1.32	1.59	2.91	1.42	1.86	0.44	2.18	1.55	-0.63
Sb_2WO_6	-0.43	-0.31	0.12	-0.34	1.72	2.06	1.93	2.34	0.41	N/A	N/A	N/A	N/A	N/A	N/A
$Co_2Mo_3O_8$	-0.69	-0.69	0	-2.27	0.03	2.24	4.29	Pri	N/A	0.55	1.57	1.02	2.03	2.03	0
$ZnCr_2O_4$	-0.46	-1.01	-0.55	-0.15	2.95	3.1	-1.1	0.64	1.74	0.81	0.74	-0.07	1.04	2.71	1.67
$LaPO_4$	-0.98	-0.62	0.36	-1.33	2.27	3.6	-2.09	0.66	2.75	0.89	3.04	2.15	1.7	2.75	1.05
Ti_3C_2O	-0.41	-0.45	-0.04	-0.67	2.6	3.27	-1.24	1.97	3.21	0.14	3.61	3.75	-1.66	3.01	4.67
ZrN	-0.76	-0.81	-0.05	0.39	2.87	2.48	-1.11	0.62	1.73	0.57	3.01	2.44	1.57	N/A	N/A
MoC	-0.44	-0.16	0.28	0.18	0.37	0.19	-0.89	0.3	1.19	0.14	2.96	2.82	1.14	2.35	1.21
NiFe LDH	0.42	-0.88	-1.3	-0.18	Pri	N/A	1.42	0.81	-0.61	2.11	0.9	-1.21	3.67	1.42	-2.25
IrO_2	-1.18	-0.82	0.36	1.5	1.39	-0.11	0.21	0.09	-0.12	0.83	0.58	-0.25	0.89	1.61	0.72
RhO_2	-0.94	-0.67	0.27	1.75	1.99	0.24	1.05	0.74	-0.31	1.92	1.46	-0.46	1.91	2.47	0.56
RuO_2	-0.7	-0.43	0.27	1.15	1.08	-0.07	0.63	0.23	-0.4	2.09	1.66	-0.43	1.62	1.8	0.18

The catalytic activities of the fourteen selected materials towards five typical electrocatalysis were also investigated on the surface before (pristine) and after coverage. The results are summarized in **Table 2**. Herein, Gibbs free energies of H_2O* (G_{H2O}), HO* (G_{HO}), COOH* (G_{COOH}), and NNH* (G_{NNH}) were selected to represent the performance of HER, ORR, CO_2RR, and NRR, respectively, while the Gibbs free energy difference between O* and HO* was to evaluate OER activity. The reason why we chose H_2O* (instead of H*) to analyze HER is because most of the TMXs are more stable in alkaline instead of acidic conditions.[15] Therefore, the adsorbed H_2O* would be a key intermediate in alkaline HER for the subsequent activation process to generate H*. The relevant computational details can be found in **Supplementary Materials**. It is worth mentioning that for the cases of nearly 1 ML occupancy, the differential binding energy of the last covered-adsorbate was calculated for consideration. Generally, it is obvious that the adsorption behavior differs quite a lot between the pristine and covered surface which further proves our findings above and verifies the significance of a prepositive surface

state study in electrocatalysis research as it can lead to a totally different but more realistic result. To note, most ΔΔG is in a positive value, indicating a weaker adsorption after coverage. While for a few cases with ΔΔG below 0, this is because of a stronger adsorption originating from the hydrogen bond formation.

Furthermore, we performed the scaling relation analysis in oxygen electrocatalysis to provide a deeper testimony of the indispensability to conduct a surface state analysis beforehand. The fitted segments of E_{HO*} *vs.* E_{O*} and E_{HO*} *vs.* E_{HOO*} are shown in **Figure 3** with the slope fixed at 1.5 and 1, respectively. In **Figure 3a**, it is clearly shown that the intercept after coverage (under ORR/OER potentials) significantly changes comparing with the pristine surfaces of TMXs (blue line), indicating a weaker O*-bonding strength under a moderate or high potential, which can be explained by previous research[11,66] that compared to radical molecules (*e.g.*, HO* and HOO*), O*-adsorption is more sensitive to the surface coverage where a more "crowded" surface would lead to stronger repulsive interactions to O* that weakens its bonding. This may lead to a significant switch of the RDS (rate-determination step) and the difference in the optimal reaction activities of ORR and OER.[11,67] For the scaling relationship between E_{HOO*} and E_{HO*}, the intercept almost remains universal. This result aligns with our previous report.[11] From the scaling relationship discovered above, we can further stress that the surface states under reaction conditions (*e.g.*, pH and potentials) should be determined before the identification and analysis of the active sites of a transition metal X-ide catalyst as it will mislead the result if overlooked. Last but not least, as this work is focused on the Prouraix diagram computing, we have made some approximations like the correction for pH and solvation effect as discussed above. Given our findings here showing the significance of the preliminary determination of surface state, future work will be focused on the comprehensive and precise computation by integrating the pH, electric, and solvation effects to give a thorough insight of this issue.

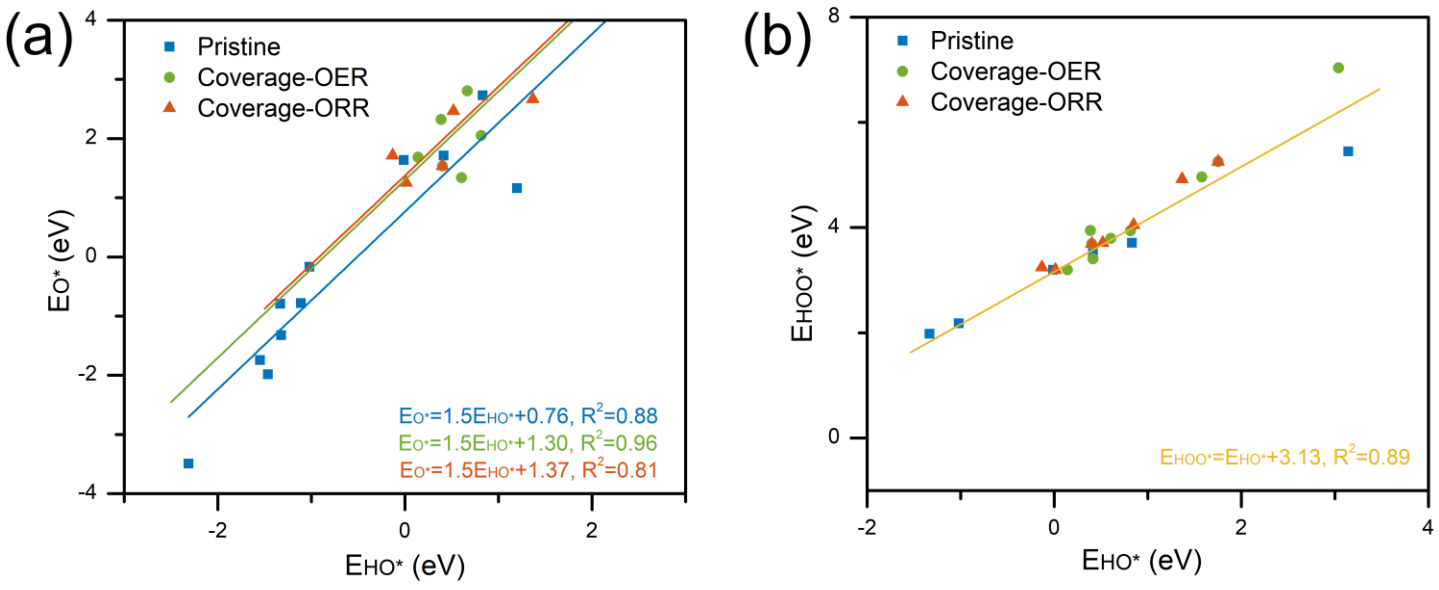

Figure 3. The scaling relations of (a) E_{HO*} *vs.* E_{O*} and (b) E_{HO*} *vs.* E_{HOO*} in oxygen electrocatalysis. The slopes were fixed at 1.5 and 1 for (a) and (b), respectively. Regression information for the linear fitting is represented by R^2.

In summary, we show that when analyzing X-ides as electrocatalysts, the surface states should not be skipped over – dismissing this important property may lead to misinterpreted reaction mechanism and active site assignment. In addition to theoretical surface Pourbaix diagram analysis, *in-situ* and post-reaction spectroscopic (*e.g.*, infrared, Raman, X-ray photoelectron, and X-ray absorption spectra) and microscopic techniques (*e.g.*, transmission electron microscope and atomic force microscope), can be coupled to provide experimental information for the description of surface properties.

Supplementary Material

See the **supplementary material** for the details of computational methods, the magnified version of **Figure 2**, and more information related to the surfaces.

Acknowledgement

This work was supported in part by the Hirose Foundation and Iwatani Naoji Foundation. We acknowledge the Center for Computational Materials Science, Institute for Materials Research, Tohoku University for the use of MASAMUNE-IMR (Project No. 202208-SCKXX-0211), the Institute for Solid State Physics (ISSP) at the University of Tokyo for the use of their supercomputers, and the assistance given by Research IT and the use of the Computational Shared Facility at The University of Manchester. Heng Liu acknowledges the China Scholarship Council (CSC, No. 202006370085) and the University of Manchester for the joint Ph.D. studentship to support his research. Hao Li and Li Wei acknowledge the University of Sydney under the International SDG Collaboration Program and the Sydney Informatics Hub (SIH), and the computation resources provided by the National Computational Infrastructure (NCI). Li Wei acknowledges the funding support from the Australian Research Council Future Fellowship (No. ARC-FT210100218). Carmine D'Agostino would like to acknowledge the EPSRC (No. EP/V026089/1) for funding his research activities. For the purpose of open access, the author has applied a Creative Commons Attribution (CC BY) license (where permitted by UKRI, 'Open Government License' or 'Creative Commons Attribution No-derivatives (CC BY-ND) license may be stated instead) to any Author Accepted Manuscript version arising.

Conflict of interests

There is no conflict of interests to declare.

Reference

[1] Z.W. She, J. Kibsgaard, C.F. Dickens, I. Chorkendorff, J.K. Nørskov, and T.F. Jaramillo, Science (1979) **355**, (2017).

[2] J.K. Nørskov, T. Bligaard, A. Logadottir, J.R. Kitchin, J.G. Chen, S. Pandelov, and U. Stimming, J Electrochem Soc **152**, J23 (2005).

[3] N.T. Suen, S.F. Hung, Q. Quan, N. Zhang, Y.J. Xu, and H.M. Chen, Chem Soc Rev 337 (2017).

[4] A. Kulkarni, S. Siahrostami, A. Patel, and J.K. Nørskov, Chem Rev **118**, 2302 (2018).

[5] D.T. Whipple and P.J.A. Kenis, J Phys Chem 3451 (2010).

[6] J.H. Montoya, C. Tsai, A. Vojvodic, and J.K. Nørskov, ChemSusChem **8**, 2180 (2015).

[7] S. Liu, H. Tao, L. Zeng, Q. Liu, Z. Xu, Q. Liu, and J.L. Luo, J Am Chem Soc **139**, 2160 (2017).

[8] Z.P. Jovanov, H.A. Hansen, A.S. Varela, P. Malacrida, A.A. Peterson, J.K. Nørskov, I.E.L. Stephens, and I. Chorkendorff, J Catal (2016).

[9] H. Tao, C. Choi, L.X. Ding, Z. Jiang, Z. Han, M. Jia, Q. Fan, Y. Gao, H. Wang, A.W. Robertson, S. Hong, Y. Jung, S. Liu, and Z. Sun, Chem **5**, 204 (2019).

[10] M. Li, H. Huang, J. Low, C. Gao, R. Long, and Y. Xiong, Small Methods **3**, 1800388 (2019).

[11] H. Li, S. Kelly, D. Guevarra, Z. Wang, Y. Wang, J.A. Haber, M. Anand, G.T.K.K. Gunasooriya, C.S. Abraham, S. Vijay, J.M. Gregoire, and J.K. Nørskov, Nat Catal **4**, 463 (2021).

[12] W. Xiong, H. Yin, T. Wu, and H. Li, Chemistry – A European Journal (2022).

[13] T. Mittermeier, P. Madkikar, X. Wang, H.A. Gasteiger, and M. Piana, J Electrochem Soc **163**, F1543 (2016).

[14] J. Seo, D. Cha, K. Takanabe, J. Kubota, and K. Domen, ACS Catal **3**, 2181 (2013).

[15] Z. Wang, Y.R. Zheng, I. Chorkendorff, and J.K. Nørskov, ACS Energy Lett **5**, 2905 (2020).

[16] Y. Wang, J. Li, and Z. Wei, J Mater Chem A Mater **6**, 8194 (2018).

[17] Y. Yuan, J. Wang, S. Adimi, H. Shen, T. Thomas, R. Ma, J.P. Attfield, and M. Yang, Nat Mater (2019).

[18] R. Luo, Z. Qian, L. Xing, C. Du, G. Yin, S. Zhao, and L. Du, Adv Funct Mater **31**, (2021).

[19] J. Hafner, J Comput Chem **29**, 2044 (2008).

[20] G. Jones, T. Bligaard, F. Abild-Pedersen, and J.K. Nørskov, Journal of Physics Condensed Matter **20**, (2008).

[21] H.A. Hansen, J. Rossmeisl, and J.K. Nørskov, Physical Chemistry Chemical Physics **10**, 3722 (2008).

[22] O. Vinogradova, D. Krishnamurthy, V. Pande, and V. Viswanathan, Langmuir **34**, 12259 (2018).

[23] H.S. Casalongue, S. Kaya, V. Viswanathan, D.J. Miller, D. Friebel, H.A. Hansen, J.K. Nørskov, A. Nilsson, and H. Ogasawara, Nat Commun **4**, (2013).

[24] W. Yang, Z. Jia, B. Zhou, L. Wei, Z. Gao, and H. Li, Commun Chem **6**, (2023).

[25] L. Zhou, H. Li, Y. Lai, M. Richter, K. Kan, J.A. Haber, S. Kelly, Z. Wang, Y. Lu, R.S. Kim, X. Li, J. Yano, J.K. Nørskov, and J.M. Gregoire, ACS Energy Lett **7**, 993 (2022).

[26] X. Zhu, X. Zhou, Y. Jing, and Y. Li, Nat Commun **12**, (2021).

[27] S. Pan, H. Li, D. Liu, R. Huang, X. Pan, D. Ren, J. Li, M. Shakouri, Q. Zhang, M. Wang, C. Wei, L. Mai, B. Zhang, Y. Zhao, Z. Wang, M. Graetzel, and X. Zhang, Nat Commun **13**, (2022).

[28] J.K. Nørskov, J. Rossmeisl, A. Logadottir, L. Lindqvist, J.R. Kitchin, T. Bligaard, and H. Jónsson, Journal of Physical Chemistry B **108**, 17886 (2004).

[29] W. Xiong, M. Zhou, X. Huang, W. Yang, D. Zhang, Y. Lv, and H. Li, Chemistry - A European Journal **28**, (2022).

[30] M. Zhou, W. Xiong, H. Li, D. Zhang, and Y. Lv, Dalton Transactions **50**, 5835 (2021).

[31] W. Xiong, M. Zhou, H. Li, Z. Ding, D. Zhang, and Y. Lv, Chinese Journal of Catalysis **43**, 1371 (2022).

[32] L. Bigiani, A. Gasparotto, C. Maccato, C. Sada, J. Verbeeck, T. Andreu, J.R. Morante, and D. Barreca, ChemCatChem **12**, 5984 (2020).

[33] T. Kishi and K. Shiota, *The Oxygen Evolution Reaction on Cobalt-Containing ~3-MnO2* (1988).

[34] H. Lin, P. liu, S. Wang, Z. Zhang, Z. Dai, S. Tan, and D. Chen, J Power Sources **412**, 701 (2019).

[35] T. Ouyang, X.T. Wang, X.Q. Mai, A.N. Chen, Z.Y. Tang, and Z.Q. Liu, Angewandte Chemie - International Edition **59**, 11948 (2020).

[36] R. Zhao, Z. Chen, Q. Li, X. Wang, Y. Tang, G. Fu, H. Li, J.-M. Lee, and S. Huang, Chem Catalysis **2**, 3590 (2022).

[37] S.G. Peera, C. Liu, A.K. Sahu, M. Selvaraj, M.C. Rao, T.G. Lee, R. Koutavarapu, J. Shim, and L. Singh, Adv Mater Interfaces **8**, (2021).

[38] Z. Zhou, Z. Yuan, S. Li, H. Li, J. Chen, Y. Wang, Q. Huang, C. Wang, H.E. Karahan, G. Henkelman, X. Liao, L. Wei, and Y. Chen, Small **15**, (2019).

[39] M. Li, H. Li, X. Jiang, M. Jiang, X. Zhan, G. Fu, J.M. Lee, and Y. Tang, J Mater Chem A Mater **9**, 2999 (2021).

[40] Y. Zhu, X. Wang, X. Zhu, Z. Wu, D. Zhao, F. Wang, D. Sun, Y. Tang, H. Li, and G. Fu, Small (2022).

[41] D.F. Abbott, S. Mukerjee, V. Petrykin, Z. Bastl, N.B. Halck, J. Rossmeisl, and P. Krtil, RSC Adv **5**, 1235 (2015).

[42] J.X. Flores-Lasluisa, F. Huerta, D. Cazorla-Amorós, and E. Morallon, Nanomaterials **10**, 1 (2020).

[43] M.M. Gomaa, G. RezaYazdi, M. Rodner, G. Greczynski, M. Boshta, M.B.S. Osman, V. Khranovskyy, J. Eriksson, and R. Yakimova, Journal of Materials Science: Materials in Electronics **29**, 11870 (2018).

[44] N. Tong, Y. Wang, Y. Liu, M. Li, Z. Zhang, H. Huang, T. Sun, J. Yang, F. Li, and X. Wang, J Catal **361**, 303 (2018).

[45] M. Han, J. Huang, S. Liang, L. Shan, X. Xie, Z. Yi, Y. Wang, S. Guo, and J. Zhou, IScience **23**, (2020).

[46] F. Almomani, R. Bhosale, M. Khraisheh, A. Kumar, and M. Tawalbeh, Int J Hydrogen Energy **45**, 10398 (2020).

[47] J.X. Flores-Lasluisa, F. Huerta, D. Cazorla-Amorós, and E. Morallón, Energy **247**, (2022).

[48] H. Miao, X. Wu, B. Chen, Q. Wang, F. Wang, J. Wang, C. Zhang, H. Zhang, J. Yuan, and Q. Zhang, Electrochim Acta **333**, (2020).

[49] F. Cheng, T. Zhang, Y. Zhang, J. Du, X. Han, and J. Chen, Angewandte Chemie - International Edition **125**, 2534 (2013).

[50] S. Luo, X. Li, W. Gao, H. Zhang, and M. Luo, Sustain Energy Fuels **4**, 164 (2019).

[51] S.R. Kelly, C. Kirk, K. Chan, and J.K. Nørskov, The Journal of Physical Chemistry C **124**, 14581 (2020).

[52] K. Chan and J.K. Nørskov, Journal of Physical Chemistry Letters **7**, 1686 (2016).

[53] A.M. Patel, S. Vijay, G. Kastlunger, J.K. Nørskov, and K. Chan, Journal of Physical Chemistry Letters **12**, 5193 (2021).

[54] I.C. Man, H.Y. Su, F. Calle-Vallejo, H.A. Hansen, J.I. Martínez, N.G. Inoglu, J. Kitchin, T.F. Jaramillo, J.K. Nørskov, and J. Rossmeisl, ChemCatChem **3**, 1159 (2011).

[55] Z.W. Ulissi, A.R. Singh, C. Tsai, and J.K. Nørskov, Journal of Physical Chemistry Letters **7**, 3931 (2016).

[56] X. Han, X. Ling, D. Yu, D. Xie, L. Li, S. Peng, C. Zhong, N. Zhao, Y. Deng, and W. Hu, Advanced Materials **31**, (2019).

[57] W. Ye, S. Chen, Y. Lin, L. Yang, S. Chen, X. Zheng, Z. Qi, C. Wang, R. Long, M. Chen, J. Zhu, P. Gao, L. Song, J. Jiang, and Y. Xiong, Chem **5**, 2865 (2019).

[58] L. Zhang, R. Si, H. Liu, N. Chen, Q. Wang, K. Adair, Z. Wang, J. Chen, Z. Song, J. Li, M.N. Banis, R. Li, T.K. Sham, M. Gu, L.M. Liu, G.A. Botton, and X. Sun, Nat Commun **10**, (2019).

[59] H. Cheng, X. Wu, M. Feng, X. Li, G. Lei, Z. Fan, D. Pan, F. Cui, and G. He, ACS Catal **11**, 12673 (2021).

[60] L. Han, Z. Ren, P. Ou, H. Cheng, N. Rui, L. Lin, X. Liu, L. Zhuo, J. Song, J. Sun, J. Luo, and H.L. Xin, Angewandte Chemie - International Edition **60**, 345 (2021).

[61] R.R. Rao, M.J. Kolb, N.B. Halck, A.F. Pedersen, A. Mehta, H. You, K.A. Stoerzinger, Z. Feng, H.A. Hansen, H. Zhou, L. Giordano, J. Rossmeisl, T. Vegge, I. Chorkendorff, I.E.L. Stephens, and Y. Shao-Horn, Energy Environ Sci **10**, 2626 (2017).

[62] A. Jain, S.P. Ong, G. Hautier, W. Chen, W.D. Richards, S. Dacek, S. Cholia, D. Gunter, D. Skinner, G. Ceder, and K.A. Persson, APL Mater **1**, 011002 (2013).

[63] P. Madkikar, D. Menga, G.S. Harzer, T. Mittermeier, A. Siebel, F.E. Wagner, M. Merz, S. Schuppler, P. Nagel, A.B. Muñoz-García, M. Pavone, H.A. Gasteiger, and M. Piana, J Electrochem Soc **166**, F3032 (2019).

[64] B.R. Wygant, K. Kawashima, and C.B. Mullins, ACS Energy Lett **3**, 2956 (2018).

[65] O. Mabayoje, A. Shoola, B.R. Wygant, and C.B. Mullins, ACS Energy Lett **1**, 195 (2016).

[66] C.F. Dickens, J.H. Montoya, A.R. Kulkarni, M. Bajdich, and J.K. Nørskov, Surf Sci **681**, 122 (2019).

[67] C.F. Dickens, C. Kirk, and J.K. Nørskov, Journal of Physical Chemistry C **123**, 18960 (2019).